

**Ultrasharp magnetization steps in the antiferromagnetic itinerant-electron system  $\text{LaFe}_{12}\text{B}_6$** L. V. B. Diop,<sup>1,2,\*</sup> O. Isnard,<sup>1,2</sup> and J. Rodríguez-Carvajal<sup>3</sup><sup>1</sup>*Université Grenoble Alpes, Institut Néel, F-38042 Grenoble, France*<sup>2</sup>*Centre national de la recherche scientifique (CNRS), Institut Néel, F-38042 Grenoble, France*<sup>3</sup>*Institut Laue-Langevin, CS 20156, F-38042 Grenoble Cedex 9, France*

(Received 17 September 2015; revised manuscript received 7 December 2015; published 26 January 2016)

The remarkable intrinsic magnetic properties of the  $\text{LaFe}_{12}\text{B}_6$  compound have been studied by neutron powder diffraction (NPD) and magnetization measurements. The NPD measurement reveals that  $\text{LaFe}_{12}\text{B}_6$  exhibits an antiferromagnetic (AFM) structure that can be described with a magnetic propagation vector of  $(\frac{1}{4}, \frac{1}{4}, \frac{1}{4})$  below  $T_N$ . In the amplitude-modulated model used for the refinement, the Fe magnetic moments are confined to the  $ab$  plane with a maximum value of  $0.43 \mu_B$  at 1.5 K. It is shown that the AFM state can be transformed to a ferromagnetic (FM) state via a field-induced first-order transition accompanied with a huge magnetic hysteresis. The  $\text{LaFe}_{12}\text{B}_6$  compound is not only the unique stable  $R\text{Fe}_{12}\text{B}_6$  phase, along the rare-earth  $R$  series but also presents unique magnetic behavior for a purely  $3d$  itinerant electron system, including particularly low ordering temperature  $T_N = 36$  K, remarkably small Fe moment, unusual amplitude-modulated magnetic arrangement, and a multicritical point in the magnetic phase diagram. In addition, we reveal that at 2 K, the AFM-FM transition is abrupt, leading to a large increase of the Fe magnetic moment up to  $1.55 \mu_B$ ; the magnetization curve presents ultrasharp steps, giving rise to an unusual staircaselike behavior.

DOI: [10.1103/PhysRevB.93.014440](https://doi.org/10.1103/PhysRevB.93.014440)

Systems exhibiting magnetic field-induced metamagnetic transitions have attracted much attention [1–11] in recent years. This metamagnetic phase transition in which the system undergoes a transition from a low magnetic moment state to a high magnetic moment state belongs to one of the most interesting magnetic phenomena [12,13]. Metamagnetic transition is observed for a variety of materials [13]. Such magnetic transition takes place at or above a certain critical field. Indeed, metamagnets present interesting properties from the technological side, as well as from the fundamental physics point of view. The most fascinating systems are those where the field-induced transition is coupled with a change in the crystal structure, giving rise to many interesting physical properties. A spectacular upsurge of interest in room temperature magnetic refrigeration has appeared worldwide due to the discovery of giant magnetocaloric effect in materials, known as metamagnets systems, such as  $\text{La}(\text{Fe}, \text{Si})_{13}$  [14] and  $\text{Gd}_5\text{Si}_2\text{Ge}_2$  [15]. Magnetic refrigeration based on the magnetocaloric effect may be a promising alternative to conventional gas-compression/expansion refrigeration due to its high energy efficiency and minimal environmental impact.

Recent investigations of the field-induced first-order transition between the antiferromagnetic (AFM) and the ferromagnetic (FM) states in the manganites that display colossal magnetoresistance have revealed unusual steplike magnetic field dependence of the magnetization and other properties measured at temperatures below 5 K [7,8,16–23]. The steps exist in both single crystal and polycrystalline samples. Note that these manganites show spontaneous jumps in magnetization and resistivity in a situation where both the magnetic field and the temperature are constant [18,20]. This kind of jump has also scarcely been observed in few rare-earth containing intermetallic compounds, such as  $\text{Gd}_5\text{Ge}_4$  [8,24–29],  $\text{Nd}_5\text{Ge}_3$  [30], and doped  $\text{CeFe}_2$  [31–33]. Most recently, steplike

transitions have been reported for  $\text{Hf}_{1-x}\text{Ta}_x\text{Fe}_2$  compounds ( $x = 0.225, 0.230, \text{ and } 0.235$ ) [34,35]. Although belonging to different classes of materials, these systems present the common features of phase-coexistence and strong magnetoelastic coupling associated with the magnetic field-induced AFM-FM transition. To explore further the generality of the observed phenomenon, we present here the existence of ultrasharp magnetization jumps at low temperature in  $\text{LaFe}_{12}\text{B}_6$  boride belonging to an entirely different class of materials.

The ternary system  $R\text{T}_{12}\text{B}_6$ , where  $R$  is a rare-earth element or yttrium and  $T$  is a  $3d$  transition metal (Co or Fe), was first identified by Niihara and Yajima [36] and later found to form with iron by Buschow *et al.* [37] during a survey of the Nd-Fe-B ternary phase diagram.  $R\text{T}_{12}\text{B}_6$  compounds crystallize in the rhombohedral  $\text{SrNi}_{12}\text{B}_6$ -type structure (space group  $R\bar{3}m$ ) [36,38,39]. The  $T$  atoms are located on two inequivalent crystallographic positions (18g and 18h) within the unit cell with the rare-earth and boron atoms occupying the  $3a$  and  $18h$  sites, respectively. Earlier reported studies on the  $R\text{Co}_{12}\text{B}_6$  systems indicate that the  $R\text{Co}_{12}\text{B}_6$  compounds are stable for essentially all of the rare-earth elements with lattice parameters that follow the lanthanide contraction [40]. By contrast,  $\text{LaFe}_{12}\text{B}_6$  is the unique stable iron-based compound of the 1-12-6 family [41–42]. It also presents unique physical properties among the  $R\text{T}_{12}\text{B}_6$  series of compounds: its Néel temperature ( $T_N = 36$  K) an order of magnitude smaller than any iron-rich  $R$ -Fe binary phase and in any case much smaller compared to the  $R\text{Co}_{12}\text{B}_6$  ferro- ( $R = \text{Y}, \text{La-Sm}$ ) or ferri- ( $R = \text{Gd-Tm}$ ) magnets ( $T_C = 134\text{--}162$  K) [40]. Even though  $\text{NdFe}_{12}\text{B}_6$  was the first iron-based example of the  $R\text{T}_{12}\text{B}_6$  series to be discovered, it is metastable. Metamagnetism in the  $\text{La}_{1-x}\text{Gd}_x\text{Fe}_{12}\text{B}_6$  borides has been investigated primarily at 4.2 K in high magnetic fields up to 35 T [42]. It has been shown that  $\text{LaFe}_{12}\text{B}_6$  is a compound with Fe moments close to magnetic instability.

In this paper, we present a detailed investigation of the magnetic properties of  $\text{LaFe}_{12}\text{B}_6$  combining microscopic

\*Corresponding author: [leopoldbirane@gmail.com](mailto:leopoldbirane@gmail.com)

(neutron diffraction) and macroscopic (magnetization) techniques. The polycrystalline sample of  $\text{LaFe}_{12}\text{B}_6$  was prepared by melting high-purity starting elements (Alfa Aesar: La, 99.9%; Fe, 99.99%; B, 99.9%) in an induction furnace under a purified argon gas atmosphere. A slight excess of La was used to avoid the presence of  $\alpha$ -Fe as the impurity phase. To promote homogeneity, the ingot was wrapped in Ta foil and then annealed at 900 °C for 3 weeks in an evacuated quartz tube. After this heat treatment, the crystallographic (phase) purity was checked by x-ray diffraction. The neutron diffraction experiments were carried out on the high-intensity powder diffractometer, D1B ( $\lambda = 2.52 \text{ \AA}$ ), at the Institut Laue-Langevin in Grenoble, France. The powder sample was contained in a vanadium cylindrical sample container. Diffraction patterns were collected over a  $2\theta$  angular range of  $128^\circ$  by using a  $^3\text{He}$  multidetector with a step of  $0.1^\circ$  between each of the 1280 detection cells. The Rietveld analysis of the neutron data was performed using the FullProf program [43], which allows the simultaneous refinement of structural and magnetic profiles. The magnetic measurements were undertaken on a free powder sample with an extraction-type magnetometer using an experimental setup that has been described elsewhere [44]. Both temperature and field dependences of the magnetization were measured in static magnetic fields up to 10.5 T at temperatures between 1.7 and 300 K.

According to the x-ray diffraction investigation, the  $\text{LaFe}_{12}\text{B}_6$  sample was found to be mainly single phase with a binary  $\text{Fe}_2\text{B}$  compound as the minority impurity phase. The analysis of the diffraction pattern confirmed that the  $R\text{-}3m$  space group symmetry is retained. The lattice parameters of  $\text{LaFe}_{12}\text{B}_6$  derived from the x-ray diffraction at room temperature are  $a = 9.631(5) \text{ \AA}$  and  $c = 7.612(1) \text{ \AA}$ , which are in good agreement with previous results [41].

For a deeper insight into the behavior of this complex system, a precise knowledge of both crystallographic and magnetic structure is required. With that aim, we have performed neutron diffraction experiments in  $\text{LaFe}_{12}\text{B}_6$ . To the best of our knowledge,  $\text{LaFe}_{12}\text{B}_6$  has not been studied using neutron diffraction; there appear to have been no direct measurements of the magnetic structure in this compound. This lack of knowledge is most probably due to the perceived difficulties associated with working with materials that contain so much highly absorbing boron ( $\sigma_{\text{abs}} = 767 \text{ b}$ ). This problem has been overcome by using  $^{11}\text{B}$  isotope in making our sample. A detailed Rietveld analysis has been performed on diffraction patterns collected at selected representative temperatures. Figure 1 shows the refinement of the pattern collected at 50 K (paramagnetic state). Fitting the 50 K diffraction pattern yields the results presented in Table I. The nuclear Bragg scattering has been fitted to the  $R\text{-}3m$   $\text{SrNi}_{12}\text{B}_6$ -type phase found at room temperature.

The diffraction pattern of  $\text{LaFe}_{12}\text{B}_6$  at 1.5 K is shown in Fig. 2. The contribution of the magnetic order to the diffraction pattern is most clearly reflected by the appearance of a new peak at a low angle ( $2\theta = 8.8^\circ$ ). The analysis of the diffraction pattern reveals that the  $\text{SrNi}_{12}\text{B}_6$ -type crystal structure is preserved down to 1.5 K. The magnetic reflections can be indexed with a propagation vector  $\mathbf{k} = (\frac{1}{4}, \frac{1}{4}, \frac{1}{4})$ . The diffraction pattern has been refined at 1.5 K on the basis

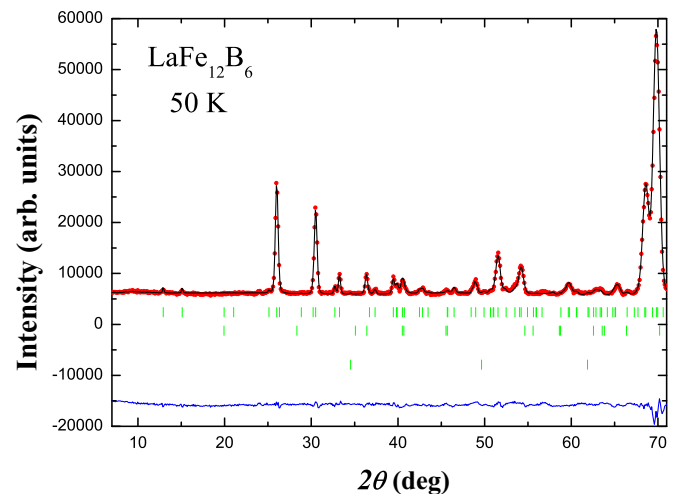


FIG. 1. Refinements of the neutron diffraction pattern for  $\text{LaFe}_{12}\text{B}_6$  taken at 50 K. The top row of the Bragg markers is for the  $\text{LaFe}_{12}\text{B}_6$  majority phase, with a second row shown for the  $\text{Fe}_2\text{B}$  impurity, and the third one corresponds to the position of the sample environment and container made of vanadium.

of an amplitude-modulated AFM structure that is depicted in Fig. 3. A summary of the crystallographic parameters and the magnetic moments obtained from the refinement are listed in Table I. The Fe magnetic moments are confined to the  $ab$  plane with a maximum value of  $0.43 \mu_{\text{B}}$  that is remarkably reduced in comparison with the elemental Fe magnetic moment of  $2.2 \mu_{\text{B}}$ . Powder neutron diffraction cannot distinguish between the orientations of the magnetic moments within the  $ab$  plane. During the refinement, we first assumed a single- $\mathbf{k}$  structure and arbitrarily fixed the direction of the magnetic moment

TABLE I. Rietveld refinement results and reliability factors obtained from the analysis of the powder neutron diffraction patterns recorded for  $\text{LaFe}_{12}\text{B}_6$  at 50 and 1.5 K.

$T$ (K)	50	1.5
$a$ (Å)	9.596(1)	9.583(1)
$c$ (Å)	7.600(1)	7.588(2)
Fe (18g)		
$x$	0.367(2)	0.367(1)
Fe (18h)		
$x$	0.424(1)	0.424(1)
$z$	0.033(1)	0.032(2)
B (18h)		
$x$	0.483(1)	0.484(1)
$z$	0.284(1)	0.283(1)
18g Fe moment ( $\mu_{\text{B}}$ )	–	0.43(3)
18h Fe moment ( $\mu_{\text{B}}$ )	–	0.43(3)
Fe moment– $c$ axis angle ( $^\circ$ )	–	90
Propagation vector	–	$(\frac{1}{4}, \frac{1}{4}, \frac{1}{4})$
$\chi^2$	9.61	9.68
$R_{\text{Bragg}}$ (%)	2.66	4.90
$R_{\text{mag}}$ (%)	–	12.4
$R_{\text{wp}}$ (%)	7.03	9.33
$R_{\text{p}}$ (%)	6.32	11.6
$R_{\text{exp}}$ (%)	2.27	3.00

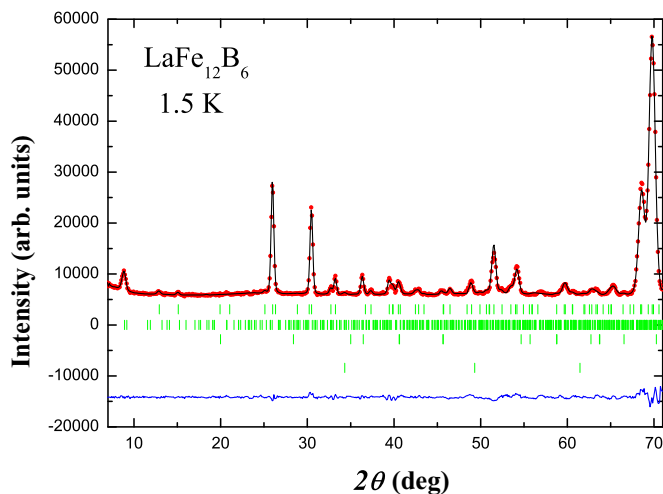


FIG. 2. Refinements of the neutron diffraction pattern for  $\text{LaFe}_{12}\text{B}_6$  taken at 1.5 K. The top and second rows of Bragg markers are referring to the nuclear and magnetic contributions of the  $\text{LaFe}_{12}\text{B}_6$  phase. The third and fourth rows are corresponding to the minority  $\text{Fe}_2\text{B}$  phase and nuclear contribution from the vanadium sample environment, respectively.

along the  $a$  axis. The establishment of an AFM structure and the weakness of the Fe moment are two noticeable results for such Fe rich compound. Note that the present magnetic structure may not be unique to account for the powder diffraction pattern. A large enough  $\text{LaFe}_{12}\text{B}_6$  single crystal would be useful to go deeper in the determination of the precise magnetic structure and distinguish among possible alternative models, such as multi- $\mathbf{k}$ .

The temperature dependence of magnetization  $M(T)$ , measured during heating of the zero-field cooled (ZFC) sample in various applied magnetic fields, is presented in Fig. 4. The  $M(T)$  measurement of  $\text{LaFe}_{12}\text{B}_6$  performed in magnetic field  $\mu_0 H = 4$  T presents a peak around 36 K and reflects the transition from an AFM phase to a typical paramagnetic (PM) state. The Néel temperature  $T_N = 36$  K found here for the  $\text{LaFe}_{12}\text{B}_6$  compound is in good agreement with that reported earlier by Li *et al.* [42]. This is a remarkably low and an unusual ordering temperature for an iron-rich compound. On heating

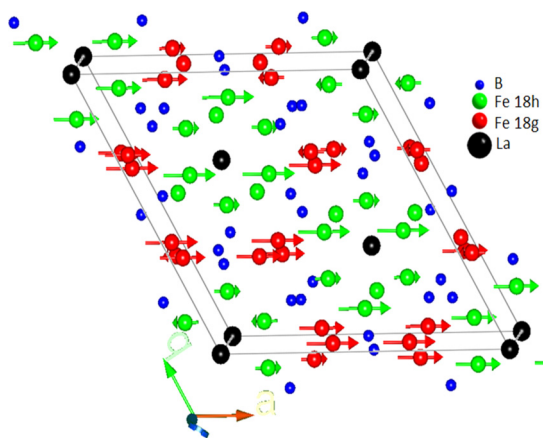


FIG. 3. Schematic representation of the amplitude-modulated magnetic structure of  $\text{LaFe}_{12}\text{B}_6$  at 1.5 K.

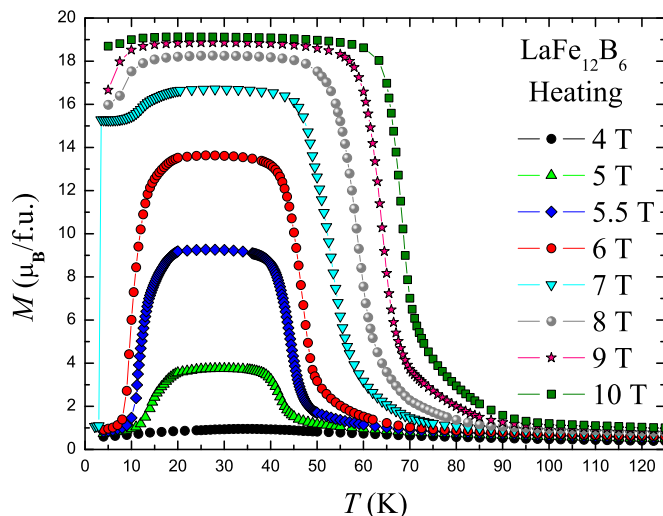


FIG. 4. Temperature dependence of the magnetization of ZFC  $\text{LaFe}_{12}\text{B}_6$  measured on heating in various applied magnetic fields.

in magnetic fields ( $\mu_0 H = 5, 5.5,$  and  $6$  T), the ZFC  $M(T)$  data of the thermally demagnetized  $\text{LaFe}_{12}\text{B}_6$  sample display a bell-like anomaly. This peculiar behavior is connected to the presence of both the low temperature AFM-FM and high temperature FM-PM transitions in the sample. Therefore, the magnetic state changes from AFM to FM and then to the PM state upon heating. The bell-like anomalies are centered at  $\approx 29$  K and a plateau develops around this temperature. Both the magnitude and the width of the plateau increase with the applied magnetic field. Note that the value of the magnetization becomes very small in the AFM state. Even more intriguing is the thermomagnetic curve measured in the magnetic field  $\mu_0 H = 7$  T: on heating from 2 K the magnetization shows a spectacular change from  $1.10$  to  $15.30 \mu_B \text{ f.u.}^{-1}$  when the temperature increases only by  $0.5$  K. The magnetization jump on the low temperature side is followed by a gradual increase in the amplitude plus a plateau, while the high temperature FM-PM transition remains continuous as in other magnetic fields. The observed discontinuity indicates a transition induced by temperature variation in magnetic field of  $7$  T. The ZFC  $M(T)$  curves in magnetic fields  $\mu_0 H > 7$  T exhibit behaviors different from those observed in low and medium magnetic fields, as shown in Fig. 4 for  $\mu_0 H = 8, 9,$  and  $10$  T. At low temperatures,  $\text{LaFe}_{12}\text{B}_6$  is basically transformed into a FM state when the magnetic field exceeds  $7$  T, except for a subtle feature still observed at the lowest temperature in the ZFC  $M(T)$  curves below  $10$  K, as illustrated in Fig. 4 for a magnetic field of  $8$  and  $9$  T. Therefore, the temperature dependence of the magnetization reflects only the FM-PM transition. All the magnetization data in the present paper were corrected for the presence of the  $\text{Fe}_2\text{B}$  impurity phase noted earlier to obtain the intrinsic  $\text{LaFe}_{12}\text{B}_6$  magnetic properties. Different methods were used to determine the amount of impurity present: (i) x-ray and neutron diffraction analysis and (ii) magnetization measurements. The latter measurements were realized just above the magnetic ordering temperature of  $\text{LaFe}_{12}\text{B}_6$  to remain far below the Curie point of  $\text{Fe}_2\text{B}$ , which is  $1015$  K. The traces of  $\text{Fe}_2\text{B}$  impurity were consequently considered

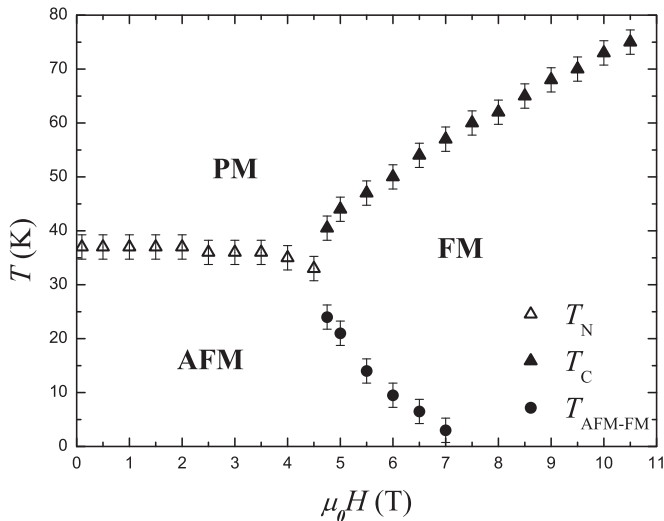


FIG. 5. Magnetic phase diagram in the field-temperature plane for the  $\text{LaFe}_{12}\text{B}_6$  compound, as derived from magnetic measurements. The Néel temperature, the Curie temperature, and the AFM-FM transition temperature are denoted by  $T_N$ ,  $T_C$ , and  $T_{\text{AFM-FM}}$ , respectively.

as carrying a saturated magnetic moment simplifying the correction for its FM contribution. The estimated impurity amounts to  $\sim 8$  wt%.

Magnetic transition temperatures were determined from the ZFC  $M(T)$  measurements displayed in Fig. 4; their values were used to construct the field-temperature  $\mu_0 H$ - $T$  magnetic phase diagram plotted in Fig. 5 for  $\text{LaFe}_{12}\text{B}_6$ . The Curie temperature  $T_C$  was determined by extrapolating the linear part of the thermomagnetic curves and finding the temperature value of the intersection with the extended baseline observed at high temperature. The magnetic transition temperature  $T_{\text{AFM-FM}}$  from the AFM to the FM state was taken as the onset of the strong increase seen on heating. The Néel temperature  $T_N$  was defined as the maximum on the  $M(T)$  curves. This phase diagram of the ZFC sample ( $T_N$ ,  $T_C$ , and  $T_{\text{AFM-FM}}$  values corresponding to those of the heating protocol) reveals the existence of multicritical point at about 4.5 T and 33 K at the crossover of the AFM, FM, and PM phase. External magnetic field was found to increase linearly the Curie temperature over the investigated field and temperature range. On increasing the external field,  $T_C$  is gradually shifted to higher temperatures at a rate of  $5.7 \text{ K T}^{-1}$ .  $T_{\text{AFM-FM}}$  decreases strongly upon increasing external field, as shown in Fig. 5. In contrast to the strong effect of an applied magnetic field on  $T_C$  and  $T_{\text{AFM-FM}}$ , the Néel temperature  $T_N$  is hardly changed by the external magnetic field. In the magnetic field range between 4.75 and 7 T (Fig. 5),  $\text{LaFe}_{12}\text{B}_6$  shows successive magnetic transitions from AFM to PM via a FM state upon increasing temperature. The field dependence of the transition temperatures points to the possibility of inducing the low temperature FM phase by applying a strong magnetic field. Note that the AFM phase persists even at a magnetic field of 7 T at 2 K. As a consequence of a strong increase of  $T_C$  with external field and a huge magnetic field induced decrease of  $T_{\text{AFM-FM}}$ , the existence domain of the FM phase of  $\text{LaFe}_{12}\text{B}_6$  increases significantly with the external magnetic field.

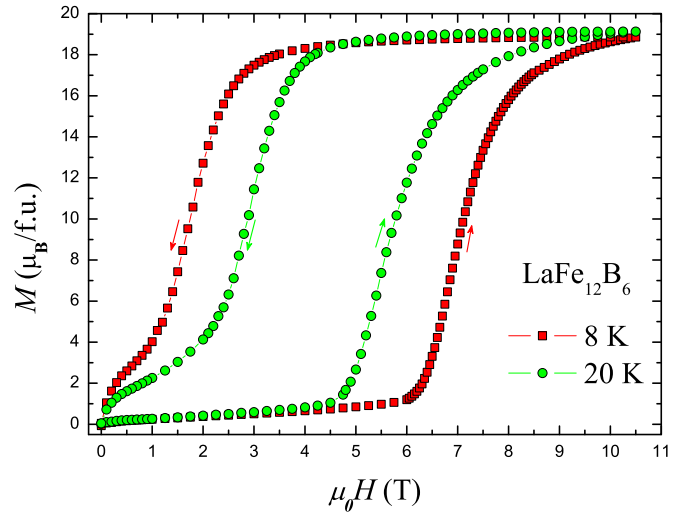


FIG. 6. Magnetization isotherms of  $\text{LaFe}_{12}\text{B}_6$  compound measured at temperature of 8 and 20 K.

To clarify the magnetic states at different temperatures and fields, isothermal magnetization measurements  $M(\mu_0 H)$  were carried out on the ZFC  $\text{LaFe}_{12}\text{B}_6$  sample. The initial magnetization data and the corresponding field-decreasing branches at 8 and 20 K are displayed in Fig. 6. The arrows indicate the magnetic field directions in which measurements have been performed. These magnetic isotherms show a field-induced metamagnetic phase transition between the AFM and FM states, which is expected in view of the  $M(T)$  data. At 8 K, the metamagnetic transition is remarkable by the huge magnetization change of about  $19 \mu_B \text{ f.u.}^{-1}$  but also by the observation of an unusually large magnetic hysteresis of 5.4 T. The Fe magnetic moment magnitude is boosted from 0.4 to  $1.6 \mu_B$  in the AFM and FM states, respectively. The hysteresis for the AFM-FM magnetic phase transition becomes smaller with increasing temperature. The observed hysteresis in the magnetization process upon increasing and decreasing fields confirms the first-order nature of the field-induced AFM-FM transition. The critical magnetic field ( $\mu_0 H_{\text{cr}}$ ) of the metamagnetic phase transition is determined as the maximum of the first derivative of the magnetic isotherms. The value of  $\mu_0 H_{\text{cr}}$  is correlated with the free energy difference between the AFM and FM states. The critical field ( $\mu_0 H_{\text{cr}}$ ) of the field-increasing branch of the AFM-FM metamagnetic transition decreases from 6.8 T at 8 K to 5.4 T at 20 K. The application of a field above  $\mu_0 H_{\text{cr}}$  is required to overcome the energy barrier between the AFM and FM states at a finite temperature. In the temperature range from 8 to 20 K, the critical transition field increases with decreasing the temperature because thermal fluctuations of the magnetic moments and/or elasticity of the lattice in the AFM state are reduced, thus enhancing negative exchange interaction [24]. Therefore, the increased negative exchange interaction raises both the free energy difference between the AFM and FM phases and the critical field required to accomplish the magnetic phase transition [24].

Magnetization isotherms in the ZFC condition have been obtained at temperatures well below 8 K. The very low temperature  $M(\mu_0 H)$  measurements show more peculiar behavior and provide useful information for the interpretation

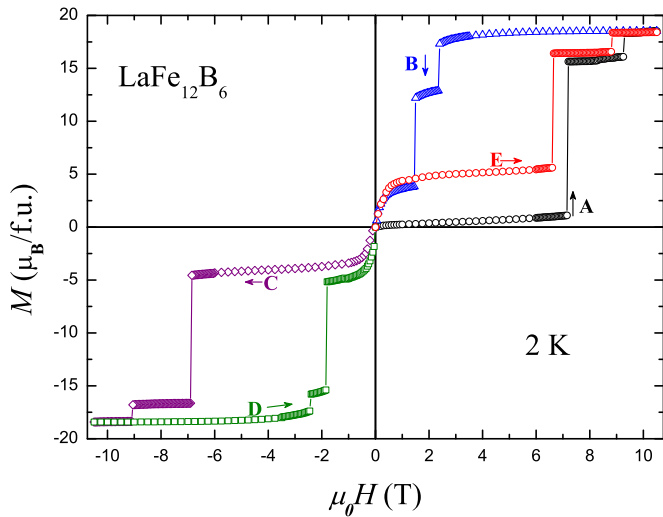


FIG. 7. Magnetization isotherm of  $\text{LaFe}_{12}\text{B}_6$  compound measured at 2 K. The arrows indicate the magnetic field directions in which measurements have been performed.

of the magnetization jump observed in the 7 T thermomagnetic curve. With lowering of the temperature, the nature of the isothermal magnetization  $M(\mu_0 H)$  plots changes drastically. An example of hysteresis cycle for  $\text{LaFe}_{12}\text{B}_6$  at 2 K is depicted in Fig. 7. In all five paths, the magnetization exhibits large discrete jumps, giving rise to a staircaselike behavior. In the first magnetization curve (path A), two ultrasharp steps are detected at  $\mu_0 H_{\text{cr}1} = 7.15$  T and  $\mu_0 H_{\text{cr}2} = 9.25$  T; the final magnetization (at 10.5 T) is the saturation value,  $M_{\text{sat}} = 18.55 \mu_{\text{B}} \text{ f.u.}^{-1}$ . The saturation value corresponds to the case of having the entire sample completely in the FM phase. One of the most striking features of  $\text{LaFe}_{12}\text{B}_6$  is that the transition between the low field AFM state and the field-driven FM state occurs via magnetic avalanches at 2 K. The multistep behavior of the magnetization can be understood if one assumes that only a fraction, 83%, of the ZFC  $\text{LaFe}_{12}\text{B}_6$  sample gets transformed into a FM state during the first step. The remaining fraction turns only at higher transition field. The hysteresis cycle shows that the forced FM state has neither magnetization remanence nor coercivity. Another noteworthy observation is that the first magnetization curve (path A) lies outside the envelope curve. Furthermore, comparing path E to path A, it is clear that when the magnetic field is reduced to zero, a fraction of the specimen volume remained FM. The increase of the FM fraction of the sample results in a larger low-field magnetization; thus, the step transitions are shifted to lower fields. The value of the critical magnetic field  $\mu_0 H_{\text{cr}}$  depends on the details of the measurement procedure and the magnetic and thermal history of the sample. In  $\text{LaFe}_{12}\text{B}_6$ , the sharp magnetization jumps are constricted to very low temperatures, vanishing for slightly higher temperatures ( $T \geq 8$  K).

As mentioned earlier, the unusual features seen in the magnetization data of  $\text{LaFe}_{12}\text{B}_6$  are very similar to those found in many phase-separated oxide manganites [7,8,16–23]. Such a distinct behavior, although common in manganese based perovskites, is very rare in the case of intermetallic compounds. There are some similarities in the behavior with rare inter-

metallics, such as  $\text{Gd}_5\text{Ge}_4$  [8,24] and  $\text{Nd}_5\text{Ge}_3$  [30]. However, the noteworthy difference that we observe in the present case as compared to many of these systems is that the multiple steps are seen not only in the first magnetization curve but in the subsequent envelope as well. This implies that the field-induced FM state loses its stability when the external magnetic field is reduced to zero. Among these systems showing the abovementioned avalanchelike behavior,  $\text{LaFe}_{12}\text{B}_6$  constitutes one of the most important examples. The origin of the steplike transitions is still a matter of controversy. Although several interpretations have been proposed by different authors for the multistep behavior in different classes of materials, the most prominent one seems to be the martensiticlike scenario driven by the applied field. Let us now try to describe the occurrence of ultrasharp and multiple steps on isothermal magnetization curves in the framework of such a martensitic scenario. The magnetic state of  $\text{LaFe}_{12}\text{B}_6$  at low temperatures and under zero field is AFM. With the application of significantly high magnetic fields, the FM phase starts growing. As the applied field is continuously increased, the driving force acting on the magnetic moments also increases. When the field is large enough to overcome the elastic constraints at the AFM/FM interfaces, the FM phase evolves catastrophically, resulting in an abrupt increase of magnetization. Along this avalanchelike process, the magnetic energy decreases, while the elastic one increases, a balance which can lead the system to be frozen in another metastable state [19]. The overall transition may thus proceed by successive jumps between metastable states (corresponding to the plateaus), which yield a staircaselike behavior on  $M(\mu_0 H)$  curves. Martensitic transformations are well known to be discontinuous; they can show burstlike effects and therefore affect strongly the magnetic properties [8]. The staircaselike behavior can be qualitatively accounted for within a martensitic scenario. We believe that the similarity of the low temperatures properties found in these completely different classes of materials (oxides and intermetallics) is not a coincidence and that the steplike transitions are manifestations of the martensiticlike nature of the transformation. In this scenario, the ultrasharp magnetization steps correspond to a burstlike growth of the FM phase within an AFM matrix.

To summarize, our neutron diffraction study on  $\text{LaFe}_{12}\text{B}_6$  has revealed an amplitude-modulated AFM structure with a propagation vector  $\mathbf{k} = (\frac{1}{4}, \frac{1}{4}, \frac{1}{4})$ . This iron-rich intermetallic compound shows several intriguing magnetic phenomena. The Néel temperature is remarkably low and unusual for an iron-rich compound. A large metamagnetic transition is shown to be field-induced from AFM to FM type order that manifests itself by a huge step of magnetization typical of a first-order transition from a low to high magnetic moment state of Fe. At the lowest investigated temperature, ultrasharp magnetization jumps are observed in the magnetic isotherm. The results of this investigation have given rise to a new magnetic phase diagram represented in Fig. 5, where the evolution of the transition temperatures is described versus field and temperature. A multicritical point is found to exist at low temperature.

The authors gratefully acknowledge the Institut Laue-Langevin for access to the neutron facility.

- [1] A. K. Pathak, D. Paudyal, W. T. Jayasekara, S. Calder, A. Kreyssig, A. I. Goldman, K. A. Gschneidner, Jr., and V. K. Pecharsky, *Phys. Rev. B* **89**, 224411 (2014).
- [2] E. Lovell, A. M. Pereira, A. D. Caplin, J. Lyubina, and L. F. Cohen, *Adv. Energy Mater.* **5**, 1401639 (2015).
- [3] B. S. Shivaram, Brian Dorsey, D. G. Hinks, and P. Kumar, *Phys. Rev. B* **89**, 161108(R) (2014).
- [4] J. Liu, D. Paudyal, Y. Mudryk, J. D. Zou, K. A. Gschneidner, Jr., and V. K. Pecharsky, *Phys. Rev. B* **88**, 014423 (2013).
- [5] J. B. Staunton, M. dos Santos Dias, J. Peace, Z. Gercsi, and K. G. Sandeman, *Phys. Rev. B* **87**, 060404(R) (2013).
- [6] M. E. Gruner, W. Keune, B. Roldan Cuenya, C. Weis, J. Landers, S. I. Makarov, D. Klar, M. Y. Hu, E. E. Alp, J. Zhao, M. Krautz, O. Gutfleisch, and H. Wende, *Phys. Rev. Lett.* **114**, 057202 (2015).
- [7] R. Mahendiran, A. Maignan, S. Hebert, C. Martin, M. Hervieu, B. Raveau, J. F. Mitchell, and P. Schiffer, *Phys. Rev. Lett.* **89**, 286602 (2002).
- [8] V. Hardy, S. Majumdar, S. J. Crowe, M. R. Lees, D. M. Paul, L. Hervé, A. Maignan, S. Hébert, C. Martin, C. Yaicle, M. Hervieu, and B. Raveau, *Phys. Rev. B* **69**, 020407(R) (2004).
- [9] L. M. Fisher, A. V. Kalinov, I. F. Voloshin, N. A. Babushkina, D. I. Khomskii, Y. Zhang, and T. T. M. Palstra, *Phys. Rev. B* **70**, 212411 (2004).
- [10] S. B. Roy, P. Chaddah, V. K. Pecharsky, and K. A. Gschneidner, Jr., *Acta Mater.* **56**, 5895 (2008).
- [11] N. V. Baranov, A. V. Proshkin, C. Czternasty, M. Meißner, A. Podlesnyak, and S. M. Podgornykh, *Phys. Rev. B* **79**, 184420 (2009).
- [12] L. J. De Jongh and A. R. Miedema, *Adv. Phys.* **23**, 1 (1974).
- [13] E. Strykowski and N. Giordano, *Adv. Phys.* **26**, 487 (1977).
- [14] V. K. Pecharsky and K. A. Gschneidner, Jr., *Phys. Rev. Lett.* **78**, 4494 (1997).
- [15] A. Fujita, S. Fujieda, Y. Hasegawa, and K. Fukamichi, *Phys. Rev. B* **67**, 104416 (2003).
- [16] S. Hebert, A. Maignan, V. Hardy, C. Martin, M. Hervieu, and B. Raveau, *Solid State Commun.* **122**, 335 (2002).
- [17] A. Maignan, S. Hebert, V. Hardy, C. Martin, M. Hervieu, and B. Raveau, *J. Phys.: Condens. Matter* **14**, 11809 (2002).
- [18] D.-q. Liao, Y. Sun, R.-f. Yang, Q.-a. Li, and Z.-h. Cheng, *Phys. Rev. B* **74**, 174434 (2006).
- [19] V. Hardy, S. Hebert, A. Maignan, C. Martin, M. Hervieu, and B. Raveau, *J. Magn. Magn. Mater.* **264**, 183 (2003).
- [20] V. Hardy, A. Maignan, S. Hebert, C. Yaicle, C. Martin, M. Hervieu, M. R. Lees, G. Rowlands, D. M. Paul, and B. Raveau, *Phys. Rev. B* **68**, 220402(R) (2003).
- [21] V. Hardy, A. Maignan, S. Hebert, and C. Martin, *Phys. Rev. B* **67**, 024401 (2003).
- [22] T. Wu and J. F. Mitchell, *Phys. Rev. B* **69**, 100405(R) (2004).
- [23] L. Ghivelder, R. S. Freitas, M. G. das Virgens, H. Martinho, L. Granja, G. Leyva, P. Levy, and F. Parisi, *Phys. Rev. B* **69**, 214414 (2004).
- [24] E. M. Levin, K. A. Gschneidner, Jr., and V. K. Pecharsky, *Phys. Rev. B* **65**, 214427(2002).
- [25] E. M. Levin, *Phys. Rev. B* **80**, 144401(2009).
- [26] E. M. Levin, K. A. Gschneidner, Jr., T. A. Lograsso, D. L. Schlagel, and V. K. Pecharsky, *Phys. Rev. B* **69**, 144428 (2004).
- [27] H. Tang, V. K. Pecharsky, K. A. Gschneidner, Jr., and A. O. Pecharsky, *Phys. Rev. B* **69**, 064410 (2004).
- [28] Y. Mudryk, D. Paudyal, V. K. Pecharsky, K. A. Gschneidner, Jr., S. Misra, and G. J. Miller, *Phys. Rev. Lett.* **105**, 066401 (2010).
- [29] Y. Mudryk, V. K. Pecharsky, and K. A. Gschneidner, Jr., *J. Appl. Phys.* **113**, 17E104 (2013).
- [30] B. Maji, K. G. Suresh, and A. K. Nigam, *Europhys. Lett.* **91**, 37007 (2010).
- [31] A. Haldar, K. G. Suresh, and A. K. Nigam, *Intermetallics* **18**, 1772 (2010).
- [32] A. Haldar, K. G. Suresh, and A. K. Nigam, *Phys. Rev. B* **78**, 144429 (2008).
- [33] S. B. Roy, M. K. Chattopadhyay, P. Chaddah, and A. K. Nigam, *Phys. Rev. B* **71**, 174413 (2005).
- [34] P. Bag, S. Singh, P. D. Babu, V. Siruguri, and R. Rawat, *Physica B* **448**, 50 (2014).
- [35] R. Rawat, P. Chaddah, P. Bag, P. D. Babu, and V. Siruguri, *J. Phys.: Condens. Matter* **25**, 066011 (2013).
- [36] K. Niihara and S. Yajima, *Chem. Lett.* **1**, 875 (1972).
- [37] K. H. J. Buschow, D. B. de Mooij, and H. M. van Noort, *J. Less-Common Met.* **125**, 135 (1986).
- [38] Yu. B. Kuz'ma, G. V. Chernyak, and N. F. Chaban, *Dopov. Akad. Nauk. Ukr. RSR Ser. A* **12**, 80 (1981).
- [39] W. Jung and D. Quentmeier, *Z. Kristallogr.* **151**, 121 (1980).
- [40] M. Mittag, M. Rosenberg, and K. H. J. Buschow, *J. Magn. Magn. Mater.* **82**, 109 (1989).
- [41] M. Rosenberg, T. Sinnemann, M. Mittag, and K. H. J. Buschow, *J. Alloys Compd.* **182**, 145 (1992).
- [42] Q. A. Li, C. H. de Groot, F. R. de Boer, and K. H. J. Buschow, *J. Alloys Compd.* **256**, 82 (1997).
- [43] J. Rodríguez-Carvajal, *Physica B* **192**, 55 (1993).
- [44] A. Barlet, J. C. Genna, and P. Lethuillier, *Cryogenic* **31**, 801 (1991).